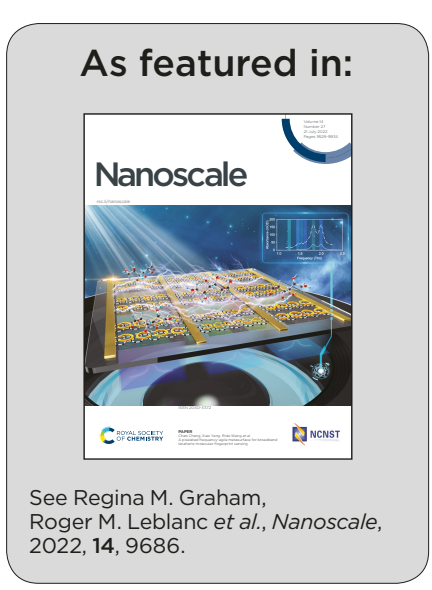


Showcasing research from the Leblanc and Graham Research Labs, University of Miami.

Surface modification of carbon nitride dots by nanoarchitectonics for better drug loading and higher cancer selectivity

Very few nanomaterials have been approved for clinical trials due to a lack of in-depth studies. This study provides a chemical and biological foundation for understanding the effects of surface functional groups of nanocarriers on their cellular uptake mechanism. The more information we have on nanomaterials, the closer they will get to real world applications. For future applications, this study opens a novel door for building personalized nanomedicine for specific cancer types by tuning the effects of surface functional groups.





Nanoscale



PAPER

View Article Online



Cite this: Nanoscale, 2022, 14, 9686

Surface modification of carbon nitride dots by nanoarchitectonics for better drug loading and higher cancer selectivity†

Emel Kirbas Cilingir, [©] ^a Meghana Sankaran, ^b Jordan M. Garber, ^a Frederic Anthony Vallejo, [©] ^{b,c} Mattia Bartoli, [©] ^d Alberto Tagliaferro, [©] Steven Vanni, ^{b,e,f} Regina M. Graham*^{b,c,g} and Roger M. Leblanc [©] *^a

Carbon Dots (CDs) have recently attracted a considerable amount of attention thanks to their well-documented biocompatibility, tunable photoluminescence, and excellent water solubility. However, CDs need further analysis before their potential use in clinical trials. Previously, we reported a new type of carbon nitride dot (CND) that displayed selective cancer uptake traits attributed to structural resemblances between CNDs and glutamine. Here, the effects of surface structural differences on the cellular uptake of CNDs are further investigated to understand their selective cancer cell uptake trend. Beyond enhanced drug loading on modified CNDs, our cytotoxicity, western blotting and bioimaging studies proposed that modified CNDs' cellular uptake mechanism is thoroughly linked with ASCT2 and LAT1 transporters. Therefore, CNDs have a promising trait of selective cancer cell targeting by utilizing highly expressed transporters on cancer cells. Additionally, drug loaded CNDs exhibited improved anti-cancer efficacies towards cancer cells along with good non-tumor biocompatibilities.

Received 14th April 2022, Accepted 31st May 2022 DOI: 10.1039/d2nr02063g

rsc.li/nanoscale

1. Introduction

Carbon dots (CDs), the latest member of the fluorescent nanomaterials family, have drawn considerable attention in the fields of cancer therapy, bioimaging, chemical sensing, and photocatalysis. Some outstanding reasons lay behind the recent interest drawn by CDs, for instance their well-documented biocompatibility, tunable photoluminescence, excellent water solubility, ease of production, and resistance to photobleaching in comparison to traditional nanomaterials. Generally, the term CDs is used to label colloidal nanoparticles

that are less than 10 nm in diameter, have a great variety of chemical functional groups at their surface, and have an sp²/sp³ hybridized carbon core.

In the literature, only a small number of existing nanomaterials have been used for clinical trials, and even fewer nanomaterials are approved for limited applications including cancer imaging and iron replacement.⁴ Cytotoxicity still remains one of the major challenges for a greater clinical translation of metal based nanoparticles and quantum dots.⁵ While traditional nanomaterials possess toxic traits, CDs are potentially safe nanocarriers since they are both highly biocompatible and water soluble. Since CDs are a recent member of the nanomaterial family, they need to be further analyzed and deeply investigated before they can be used in clinical trials.

With swift advances in both the fields of genomics and translational research, mankind has pioneered an opportunity to understand the chemical and biological fundamentals of cancer by translating these laboratory discoveries into personalized medicine. Kathleen Sebelius, the former secretary of Health and Human Services, mentioned their goals related to personalized medicine, which are "when doctors can truly prescribe the right treatment, to the right person, at the right time, we will have a new level of precision and effectiveness that will provide the knowledge-driven power that is necessary to achieve our highest goals in healthcare reform, including

^aDepartment of Chemistry, University of Miami, 1301 Memorial Drive, Coral Gables, Florida 33146, USA. E-mail: rml@miami.edu;

Tel: +1 (305) 284-2194; Locater code: 0431

^bDepartment of Neurosurgery, University of Miami Miller School of Medicine, 1095 NW 14th Terrace, Miami, FL 33136, USA. E-mail: rgraham@med.miami.edu; Tel: +1 (305) 321-4972

^cUniversity of Miami Brain Tumor Initiative, Department of Neurosurgery, University of Miami Miller School of Medicine, 1095 NW 14th Terrace, Miami, FL 33136, USA ^dDepartment of Applied Science and Technology, Politecnico di Torino, Italy

^eHCA Florida University Hospital, 3476 S University Dr., Davie, FL 33328, USA ^fDr. Kiran C. Patel College of Osteopathic Medicine, Nova Southeastern University, 3301 College Avenue, Fort Lauderdale, Florida 33314-7796, USA

^gSylvester Comprehensive Cancer Center, University of Miami Miller School of Medicine, 1475 NW 12th Ave. Miami. FL 33136, USA

[†] Electronic supplementary information (ESI) available. See DOI: https://doi.org/ 10.1039/d2nr02063g

Nanoscale Paper

more effective disease prevention and early disease detection". Despite many examples of tailoring treatments using genetics for patients with various cancers, the successful implementation of personalized medicine must assess factors beyond genetic information. It is required to incorporate new vet fundamental chemical and biological findings to advance these discoveries towards clinical applications.^{8,9}

Our group previously reported about the synthesis of carbon nitride dots (CNDs) as a targeted cancer therapy and selective bioimaging nanomaterial. 10 Urea and citric acid were chosen as precursors for the synthesis of CNDs. In vitro bioimaging studies using pediatric glioma cells (SJ-GBM2) were performed to analyze the possible selective biolabeling and biodistribution within the cell membrane. Overall, CNDs selectively entered SJ-GBM2 tumor cells more efficiently, while cellular uptake was noticeably lower for normal human embryonic kidney cells (HEK293). We hypothesized that this observation was related to high surface structural resemblance of CNDs to the amino acid glutamine. To sustain rapid cell proliferation, cancer cells undergo metabolic reprogramming leading to an increased need for amino acids compared to non-cancer cells. Glutamine is especially important for biosynthesis, energy production and redox homeostasis and as such cancers can become "addicted" to glutamine.11 This dependence on glutamine may be considered cancers' Achilles heel; therefore, developing a CND nanocarrier targeting the glutamine transporters should increase the specificity toward cancer cells and thus, the efficiency of drug delivery.

To test and develop the previous hypothesis further, we modified the surface functional groups of CNDs to analyze their properties regarding selective cellular uptake of cancer cells. We, consequently, were able to manipulate the amount of surface primary amine and carboxylic groups. By changing the precursors' ratios at the beginning of the synthesis, we have synthesized CNDs with different ratios of surface functional groups. After meticulous characterization of these modified CNDs, we conjugated doxorubicin (a very well-known cancer drug) onto the modified surface of CNDs. The doxorubicin conjugated CNDs were, subsequently, treated on different pediatric high-grade gliomas including glioblastoma (GBM) and diffuse intrinsic pontine glioma (DIPG), and highrisk neuroblastoma cell lines. According to our cell viability studies, the surface modified CNDs were able to carry more doxorubicin with exceptional cancer toxicity in addition to preserving their biocompatible traits towards non-tumor cells. Moreover, to further analyze the cancer cell uptake of the surface modified CNDs, we employed bioimaging studies with 5 different inhibitors. Our bioimaging results suggested that the cellular uptake mechanism of modified CNDs is highly related to the expression levels of amino acid transporters, specifically ASCT2 and LAT1. ASCT2 is the preferred amino acid transporter for glutamine while LAT1 preferentially transports large branched and aromatic neutral amino acids, such as tryptophan (Fig. 1). Both ASCT2 and LAT1 are overexpressed in a wide range of tumors. 12 Although more analysis and investigation of their characteristics are still needed, CNDs appear

extremely promising as versatile nanocarriers for future clinical trials of cancer.

2. Experimental section

Materials used

Anhydrous citric acid (purity >99.5%), urea, doxorubicin hydrochloride >95% (by HPLC), N-hydroxy succinimide (NHS), 1-ethyl-3-(3-dimethylaminopropyl) carbodiimide hydrochloride (EDC), dithiothreitol (DTT), and lactic acid were purchased from VWR (West Chester, PA), Eastman Kodak Company (NY, U.S.A.), Sigma Aldrich (St Louis, MO), respectively. Deionized (DI) water was used for preparing all of the solutions and dialysis of carbon dots. A MilliQ3 water purification system obtained from Millipore Sigma (Burlington, MA) was employed to purify water. The surface tension of the purified deionized water was calculated to be 72.6 mN m⁻¹ with a resistivity of 18 MΩ cm, and a pH value of 6.6 \pm 0.3 at 20.0 \pm 0.5 °C. Spectra pore dialysis tubing with a molecular weight cutoff (MWCO) of 100-500 Da was purchased from VWR (West Chester, PA) and used for dialysis. The pediatric glioblastoma cell line SJ-GBM2 and the MYCN amplified neuroblastoma cell line SMS-KCNR were obtained from the Children's Oncology Group (COG, Texas Tech University, Health Science Center, TX, USA). Pediatric glioblastoma cell lines SF188 and KNS42 were generously provided by Dr Chris Jones (Paediatric Oncology, The Institute of Cancer Research, Sutton, United Kingdom). SJ-GBM2, SMS-KCNR, SF188 and KNS42 were maintained in RPMI media supplemented with 10% FBS and 1% pen/strep (Gibco, Carlsbad, CA). The diffuse pontine glioma (DIPG) cell line NP53 was kindly provided by Dr Oren Becher (Northwestern University Feinberg School of Medicine, Ann and Robert H. Lurie Children's Hospital of Chicago Illinois, USA). This cell line was derived from a mouse DIPG model induced by PDGF-B signaling, TP53 loss, and ectopic H3.3K27 expression.¹³ DIPG cells were cultured in Complete NeuroCultTM Proliferation Medium (Stemcell Technologies, Vancouver, Canada) supplemented with 1% pen/strep. Mesenchymal stem cells (MSCs) originally derived from human bone marrow aspirates were obtained from Thermo Fisher Scientific and maintained in MEM alpha supplemented with 20% FBS and 1% pen/strep. Prior to drug treatment, MSCs were moved to media with 10% FBS. All cells were maintained at 37 °C in a humidified 5% CO2 incubator and routinely tested for mycoplasma using a LookOut mycoplasma PCR detection kit (Sigma Aldrich, St Louis, MO). To guard against excessive cell passaging, newly received cell lines were routinely expanded with several cryovials frozen down for future use. The cell lines utilized in this study are not listed in the most recent NCBI database for misidentification and contamination of human cell lines.

Synthesis of 1:1, 1:3 and 1:5 CNDs

Carbon-nitride dots with different ratios of citric acid to urea were synthesized by following Liyanage et al. using a hydroPaper Nanoscale

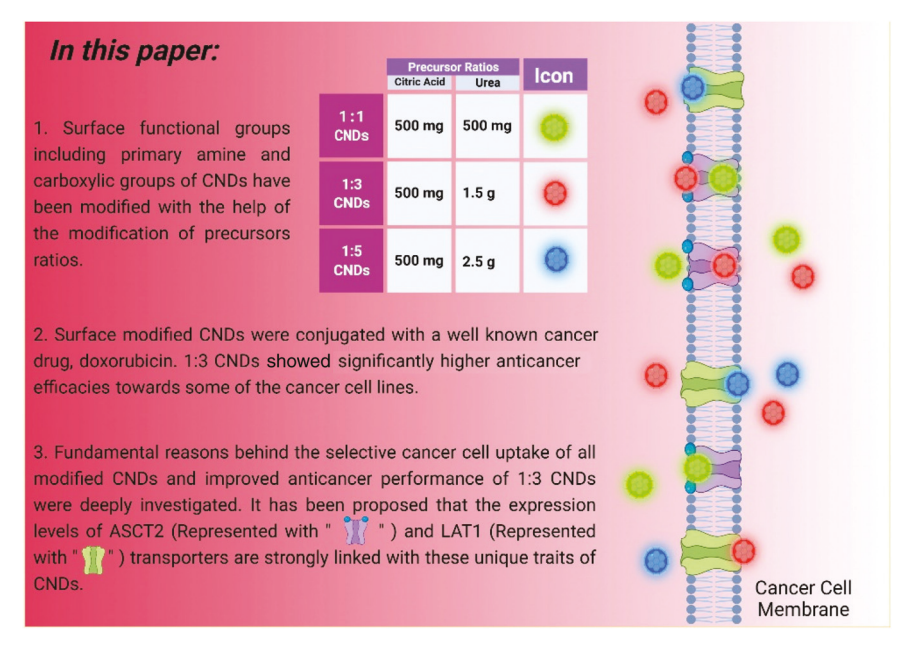


Fig. 1 Highlights of this manuscript.

thermal microwave-mediated procedure. ¹⁰ Briefly, 0.5 g of citric acid and 0.5, 1.5 and 2.5 g of urea were dissolved in 25 mL of DI water for the preparation of the 1:1, 1:3 and 1:5 CND ratios, respectively. This mixture was left to stir vigorously overnight. Then the mixture was heated for 7 min (700 W) until all the water evaporated and the mixture turned into a black solid product. 15 mL of DI water was added on top to disperse the product and sonicated for 30 min. Then the dispersed CD solution was centrifuged for 15 min at 1500 rpm twice to get rid of any precipitation. The supernatant was further purified *via* syringe filtration with a filter membrane of 0.2 µm. The filtrate was dialyzed against DI water for 3 days using 100–500 Da MW cutoff dialysis tubing. As the final step, the water remaining after dialysis was evaporated using a rotavapor by heating to 70–80 °C.

2.3. Characterization of the CND ratios

The prepared CNDs were characterized by UV-vis absorption in a 1 cm quartz cuvette (Starna Cells) using a Cary 100 UV-vis spectrophotometer (Agilent Technologies) in an aqueous medium. A Horiba Jobin Yvon Fluorolog-3 with a slit width of 5 nm was used for obtaining the photoluminescence emission spectra of the CND ratios along with using a 1 cm path length quartz cuvette. Fourier Transform Infrared (FTIR) spectra were recorded using a PerkinElmer Frontier with a universal ATR sampling accessory using air as the background. Mass spectroscopy was performed with a Matrix-Assisted Laser Desorption/Ionization-Time of Flight (MALDI-TOF) mass spectrometer (MS) using a Bruker auto flex speed spectrometer. AFM studies were conducted using an Agilent5420 atomic force microscope in the tapping mode. TEM studies were performed with a JEOL 1200× TEM. For the zeta potential measurement, a DLS nano series Malvern Zetasizer

(Westborough, MA) was employed. XPS spectra were recorded using a PHI 50 0 0 Versaprobe (Physical Electronics, Chanhassen, MN, USA) scanning X-ray photoelectron spectrometer (monochromatic Al K-alpha X-ray source with 1486.6 eV energy, 15 kV voltage, and 1 mA anode current). For the quantification of doxorubicin loading, circular dichroism (CD) analyses were performed using a JASCO J-810 spectropolarimeter within the range of 275 to 550 nm using 1 cm quartz cells (Starna Cells, Inc.; Atascadero, CA). Three batches of CNDs were analyzed by repeating each characterization method.

2.4. Surface functional group quantification

We implemented fluorescence analysis using the fluorescamine assay to calculate the number of primary amine groups on the surface of modified CNDs. A published process has been followed to perform this work. Heriefly, 2 mg of modified CNDs was dispersed in 2 mL of acetone/1× PBS (1:1) buffer solution. The prepared solutions of CND ratios were diluted 100 times to prevent future errors caused by emission saturation. Upon addition of 1,2-ethylenediamine (EDA) into fluorescamine, we analyzed the linear relationship between the molarity of primary amine groups and the fluorescence intensity of the solutions. The acquired fluorescence intensity from the addition of fluorescamine into modified CND aqueous dispersion was incorporated into the linear equation relationship. From this equation, quantification of primary amine groups on 2 mg of modified CNDs was calculated.

We employed a classical acid-base titration to quantify the number of carboxylic groups on the surface of modified CNDs. 0.5 mg mL⁻¹ stock solution of modified CNDs was prepared. Then, this stock solution was diluted to 0.02 mg mL⁻¹ concentration. The titration of these solutions was performed with

Nanoscale Paper

the slow addition of 50 mL of 0.005 mol $\rm L^{-1}$ NaOH solution along with inserting the probe of the SCHOTT Lab 850 benchtop pH meter. Titration was conducted until the pH meter shows a pH value of around 7 for over 3 min waiting time. Finally, the volume of added NaOH solution was recorded for the calculation of the carboxylic groups on modified CNDs.

2.5. Fluorescence quantum yield calculations

We calculated the fluorescence quantum yield (Φ) of CNDs by comparing the integrated area under the fluorescence curve and the absorbance intensity values using quinine sulfate and harmane as the reference standards. In the literature, quinine sulfate and harmane have 54% and 83% quantum yield (QY), respectively, when they are dissolved in 0.1 M H₂SO₄ (refractive index, $n_R = 1.33$, at 350 nm). ¹⁵ We dispersed modified CNDs in DI water (refractive index, $n_R = 1.33$). Then, the prepared solutions of CNDs were analyzed with UV-vis absorbance in a 1 cm path length quartz cuvette. The absorbance intensity was maintained under 0.05 a.u. and absorbance data were collected at 350 nm. Subsequently, the fluorescence emission spectra of some solutions of modified CNDs were obtained with the 350 nm excitation wavelength. The average of 5 repeats of absorbance intensities and integrated areas for the fluorescence emission spectra were fitted in the following equation,

$$\Phi = \Phi_{\rm R} \times (I/I_{\rm R}) \times (A_{\rm R}/A) \times (n^2/n_{\rm R}^2) \tag{1}$$

In this equation, Φ_R , I, A, and n symbols correspond to the literature QY of the standard, the integrated area under the PL curve, the absorbance intensity at 350 nm, and the refractive index, respectively. Sub-script R is denoted for the reference.

2.6. Conjugation of doxorubicin on CNDs

6 mg of 1:1, 1:3, and 1:5 CNDs were dissolved in 2 mL of PBS (7.4 pH) solution. Then, 12.9 mg of 1-(3-dimethylaminopropyl)-3-ethylcarbodiimide hydrochloride (EDC) was dissolved in 1 mL of DI water and added to the CND solution. The mixture was stirred at room temperature for 30 min. Then, 9.8 mg of *N*-hydroxysuccinimide (NHS) dissolved in 1 mL of DI water was mixed into the solution. After 30 min of stirring, 4.6 mg of doxorubicin dissolved in 1 mL of dimethyl sulfoxide (DMSO) was added to the solution. The entire mixture was stirred at room temperature overnight. Then the mixture was dialyzed by using a 100–500 Da MWCO dialysis bag for 3 days. DI water was replaced every 4–10 h. Finally, the frozen samples were lyophilized for 3 days to obtain the powdered product.

2.7. Cell viability studies

At 24 h prior to treatment, cells were seeded at a density of either 0.5×10^5 cells per ml (MSC), 1×10^5 cells per ml (SJ-GBM2, SMS-KCNR, KNS42) or 1.5×10^5 cells per ml (SF188 and NP53) in 100 μ L in 96-well plates. Next, the cells were treated with 100 μ L of different concentrations (0, 40, 80, 200, 400 nM) of 1:1, 1:3, and 1:5 CNDs. The cells were also treated with 100 μ L of different concentrations (10, 50, 100,

250 nm) of doxorubicin. Treatment was assessed either after 72 h of exposure or 3 h of exposure during which CNDs and doxorubicin were removed and replaced with fresh media. Cell viability was determined using the CellTiter 96 Aqueous One Solution Cell Proliferation Assay (MTS) (Promega Madison, WI). The absorbance was measured at 490 nm using a BioTek Synergy HT plate reader. An average of 3 separate experiments were performed to present the data in which viability was calculated as the relative percentage of non-treated cells. Finally, the standard error of the mean (SEM) was also computed for viability results.

2.8. Western blotting

For western blotting studies, we followed our previous protocol that has been published. 16 MSC, SJ-GBM2, SF188, SMS-KCNR, KNS42, and NP53 cells were lysed in RIPA buffer and protein concentrations were calculated using BCA protein assay (BioRad Hercules, CA). Equal amounts of protein (20 µg) were loaded onto 12 polyacrylamide gels (BioRad Hercules, CA) for electrophoresis and subsequently transferred onto nitrocellulose membranes. Then, these membranes were blocked for 1 h in 5% non-fat milk (Biorad, Hercules, CA) at room temperature (RT) and incubated with the primary antibody diluted in 2.5% BSA overnight at 4 degrees. ASCT2 transporter polyclonal antibodies (SLC1A5) and LAT1 transporter polyclonal antibodies (SLC7A5) were obtained from MyBioSource (San Diego, CA), Invitrogen (Waltham, MA). Finally, all membranes were incubated at room temperature with anti-mouse or anti-rabbit secondary antibodies for 1 h. Blots were processed using SuperSignalTM West Pico Chemiluminescent (Thermo Scientific Waltham, MA).

2.9. In vitro bioimaging

MSCs and SJ-GBM2 cells were plated in 4-well plates (NUNC, Denmark) for imaging and incubated for 24 h for sufficient cell growth. Then, the media were removed; the cells were treated with 500 μL of serum free DMEM and RPMI solutions containing 1 mg mL $^{-1}$ 1:1, 1:3, and 1:5 CNDs and further incubated for 1 hour. After this treatment, cells were washed with PBS and treated with 1 μg mL $^{-1}$ Hoechst for 15 min. Then, cells were washed with PBS two more times and fixed with 4% formaldehyde for 20 min. After fixation, 100 μL of Citifluor antifade agent was added to the cells for 2 days. Finally, the cells were washed with PBS three times to wash off the antifade agent. The cells were subjected to fluorescence microscopy imaging using a Floid Cell Fluorescent Microscope (Thermo Fisher Scientific, Waltham, MA). The same imaging settings were used for each group.

Additional bioimaging studies were performed with the presence of 5 different ASCT2 and LAT1 transporter competitive ligands. The ASCT2 transporter inhibitors, *O*-benzyl-pserine (Benser), glutamine, (2*S*)-2amino-4-[bis[[2-[(3-methyl-phenyl)methoxy]phenyl]methyl]amino]-butanoic acid (V-9302) were purchased from Chemcruz (Dallas, TX), Gemini Biosciences (West Sacramento, CA), and Cayman Chemical (Ann Arbor, MI), respectively. The LAT1 transporter inhibitors

Paper Nanoscale

2-amino-bicyclo [2.2.1]heptane-2-carboxylic acid (BCH) and tryptophan were obtained from Gemini Biosciences (West Sacramento, CA), and Cayman Chemical (Ann Arbor, MI). The glioblastoma S-IGBM2 (1 \times 10⁵) cells were divided into 4-well plates (NUNC, Denmark) for inhibitor imaging studies in 750 µL media and incubated for 24 h for sufficient cell growth. On the next day, the cell media were aspirated, and the cells were pretreated with inhibitors: Benser (60 mM), glutamine (60 mM), V-9302 (15 μM), BCH (15 mM), and tryptophan (60 mM) for 15 min. After this treatment, 500 µL DMEM and RPMI solutions containing 1 mg mL⁻¹ 1:1, 1:3, and 1:5 CNDs were added to cells and incubated for 1 hour. Then, the cells were washed with PBS 2 more times and fixed with 4% formaldehyde for 20 min. After fixation, 100 µL of the Citifluor antifading agent was added to the cells and incubated for 2 days. Finally, the cells were washed with PBS 3 more times to wash off the antifading agent. The cells were imaged by fluorescence microscopy using a Floid Cell Fluorescent Microscope (Thermo Fisher Scientific, Waltham, MA). The same imaging settings were used for each group.

2.10. Image analysis

The image analyses of modified CNDs were performed using ImageJ v.1.53i. PL intensity quantification analyses of images were performed using Graphpad Prism 9.3.1 software. The pixel counts per fluorescence intensity (grey scale) quantification of fluorescence intensities of cells were determined using ImageJ v.1.53i. The relative pixel count is the number of pixels with a given fluorescence intensity within a selected region of interest (either MSC or SJ-GBM2 cells), subtracted by the background pixels in that region. PL intensities are represented as a box plot. In boxplots, center bars represent medians and expand to the first and third quartiles; whiskers extend to min/max data points. Statistically significant differences of PL intensities of images were determined using oneway analysis of variance (ANOVA) $(P \le 0.001)$ followed by Tukey's honest significant difference *post hoc* test ($P \le 0.05$).

2.11. Statistical analysis

The significance of cytotoxicity and cell viability studies was calculated by performing Student's t-tests for all pairwise comparisons of the different treatments that were tested. All the results are presented as the mean ± standard error of the mean (SEM). Significance was set at $p \le 0.05$.

3. Results

Characterization of 1:1, 1:3, and 1:5 CNDs

Our main goal was to modify the surface of CNDs for a larger investigation of their chemical and biochemical characteristics. It is for this reason that we have used different proportions of precursors to synthesize CNDs. The modified CNDs were first characterized using UV-vis absorption spectra. Modified CNDs exhibited characteristic bands in the range of 200-400 nm (Fig. 2A). Previously, these bands were assigned to

n- π^* electronic transition of C=O groups and π - π^* electronic transition of carbon nitride s-triazine rings. 10 On the other hand, both 1:3 and 1:5 CNDs presented a more prominent band at 412 nm, which was assigned to the $n-\pi^*$ electronic transition of C-N and C=N groups. 17 Furthermore, 1:3 and 1:5 CND spectra show the same absorption bands for the π - π * electronic transition of C=C groups and the n- π * electronic transition of C=O groups at 252, 271, 327, and 335 nm wavelengths. When we analyzed the PL emission spectra of 1:3 and 1:5 CNDs, we noticed some differences compared to 1:1 CNDs. For instance, there was a red shift in the emission bands excited at 350 and 375 nm. Fig. 2B shows the PL emission spectrum of 1:1 CNDs and maximum peaks for emission bands excited at 350 and 375 nm are at 442 and 483 nm, respectively. Differing from the emission bands of 1:1 CNDs, the 1:3 PL peaks are observed at 498 and 507 nm for the same excitation wavelengths (Fig. 2C); 1:5 CNDs produce PL maximum peaks at 501 and 507 nm for the same excitation wavelengths (Fig. 2D). All three types of CNDs have excitation dependent emission properties which are observed from the normalized PL spectra. Currently, there is no agreement with the mechanism behind the excitation dependent PL behavior of CDs. Moreover, the most prevalent theories behind this behavior were attributed to the presence of surface electronic states, the incorporation of fluorophores into the particle structure, and dot-to-dot variations, which ultimately led to the excitation-dependent ensemble properties. 18 We observed distinct differences between the FTIR bands between 1:1, 1:3 and 1:5 CNDs (Fig. 2E). Firstly, both 1:3 and 1:5 CNDs had significant decreases in the prominence of the 3026 cm⁻¹ band, which was assigned to $\nu_{\text{O-H}}$ from the -COOH groups. This result presented the first confirmation that there is a decrease in the amount of -COOH groups in the modified 1:3 and 1:5 CNDs. Conversely, another imperative finding was observed at the 1690 cm⁻¹ band. This band was assigned to $\nu_{\rm C=O}$ of amide functional groups. Both 1:3 and 1:5 CNDs showed more prominent amide bands than 1:1 CNDs. In other words, there was an increase in the amount of -NH2 groups on both 1:3 and 1:5 CNDs. The remaining FTIR bands peaking at 3185, 2761, 1776, 1592, 1414, 1361, 1290, 1181, 1047, and 766 cm⁻¹ were assigned to ν_{N-H} , ν_{O-H} , $\nu_{C=O}$, $\delta_{\text{C-H}}$, $\delta_{\text{O-H}}$, $\nu_{\text{C-O}}$, $\nu_{\text{C-N}}$, $\nu_{\text{C-O}}$ and s-triazine, respectively. 15,19,20

We have investigated morphological and size distribution properties of modified CNDs by AFM and TEM studies. In our previous study, we mentioned that 1:1 CNDs retain a height profile between 1.0 and 3.8 nm and a diameter ranging between 2.0 and 3.5 nm.10 The height of 1:3 CNDs is in the range of 1.6-2.0 nm (Fig. S1A†) while their average diameter is between 2.7-3.1 nm (Fig. S1B†). For the 1:5 CNDs, they had a height profile between 1.3 and 2.1 nm and the average diameter between 2.7 and 3.2 nm (Fig. S1C and D†). Both the 1:3 and 1:5 CNDs present similar height profiles to their average diameters, verifying a spherical shape in general. In summary we did not notice a relevant change in the morphology and size of CNDs when the ratio of urea to citric acid varied.

Nanoscale Paper

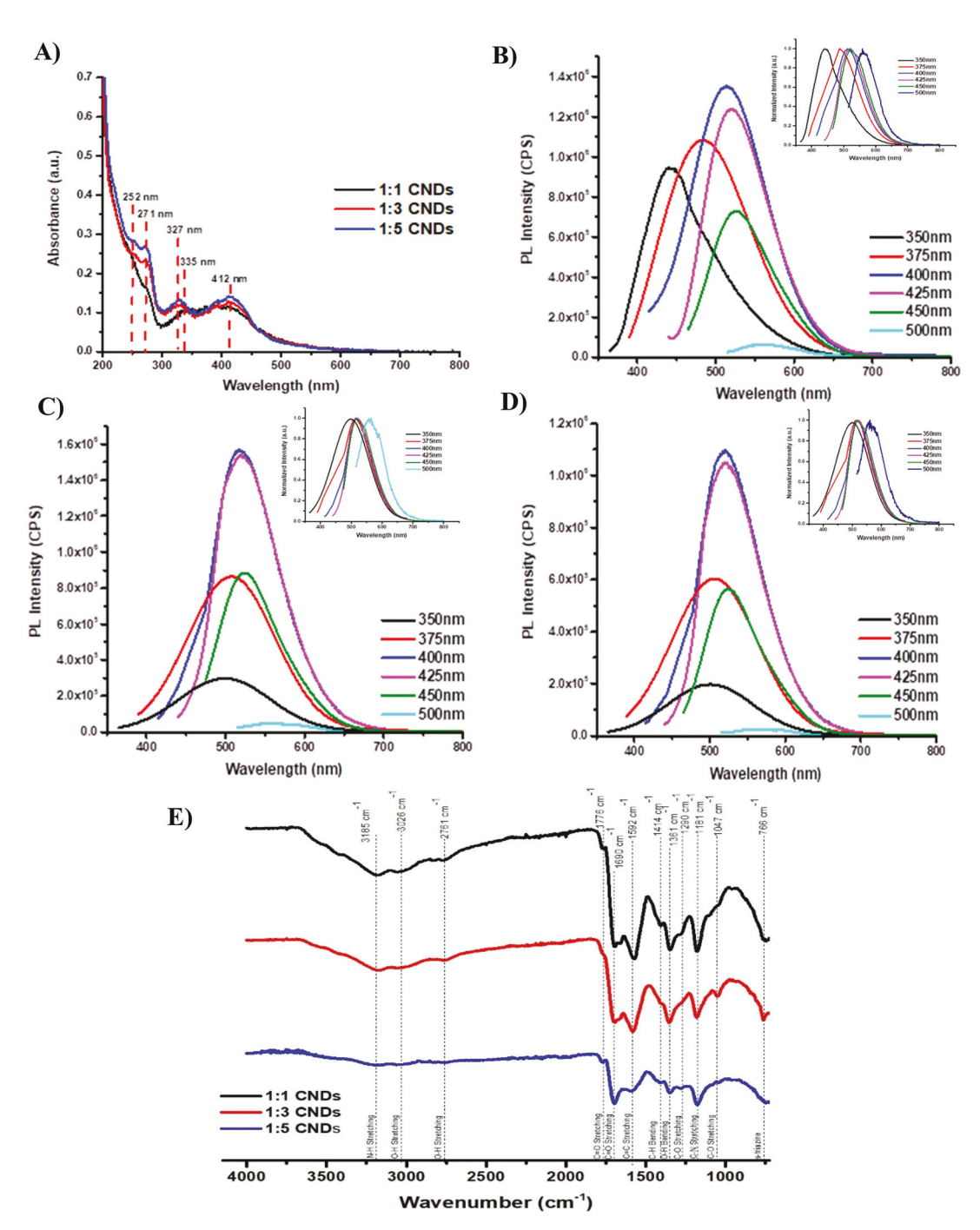


Fig. 2 (A) UV-vis absorption spectra of modified CNDs (concentration = 0.1 mg ml $^{-1}$). (B-D) PL emission spectrum of 1:1, 1:3, 1:5 CNDs (concentration = 1 × 10 $^{-6}$ mg ml $^{-1}$), respectively. Insets, normalized PL emission spectra of 1:1, 1:3, 1:5 CNDs. (E) FTIR spectra of modified CNDs.

To further characterize the modified CNDs, we calculated the quantum yield (QY), quantified the amount of surface –COOH and $-NH_2$ groups, found the surface charge, and obtained the MALDI-TOF main +1 ionization peak for 1:1, 1:3 and 1:5 CNDs (Fig. 3A). Accordingly, we have measured the QY of the three types of modified CNDs, but we did not observe a drastic change in their brightness. The original CNDs (1:1) had a QY of around 11.53% while modified 1:3

and 1:5 CNDs showed QY values of 12.54% and 9.53%, respectively. To assess the variations in the amount of surface –COOH and –NH₂, we employed a straightforward acid–base titration and a fluorescamine assay. As a result, we obtained further confirmation that the amount of surface –COOH groups is less in both the 1:3 and 1:5 CNDs than the 1:1 CNDs (Fig. 3A). For each gram of 1:1, 1:3 and 1:5 CNDs, there were 0.3, 0.2, and 0.184 mmol of –COOH groups, respect-

A) Sample	QY (%) ± STD	Number of - COOH groups on the surface (mmol/g)	Number of - NH ₂ groups on the surface (mmol/g)	Zeta Potential (mV)	MALDI-TOF +1 Ionization Main Peak (m/z)	
1:1 CNDs	12 ± 2.0	0.30	0.007	-38.8	750	
1:3 CNDs	12 ± 2.1	0.20	0.010	-23.4	750	
1:5 CNDs	10 ± 1.8	0.18	0.024	-20.4	750	

B)	Carbon Species (%)				Oxygen Species (%)			Nitrogen Species (%)		
Sample	C sp ²	C-X	C=O	СООН	-OH	C=O	СООН	N	NH ₂	NQ
_		(X= N, O)						Pyridinic		
1:1 CNDs	54	17	24	5	4	78	18	17	50	33
(C: 64%, O:										
24%, N: 12%)										
1:3 CNDs	56	16	24	4	14	69	17	21	55	24
(C: 65%, O:										
22%, N: 13%)										
1:5 CNDs	58	15	24	3	3	81	16	22	57	21
(C: 66%, O:										
21%, N: 13%)										

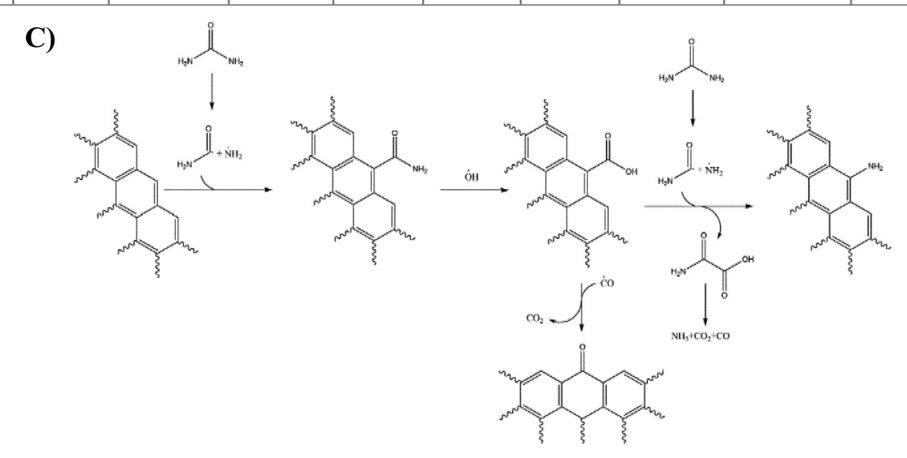


Fig. 3 (A) Table for quantum yield, number of -COOH and $-NH_2$ groups on the surface, surface charge and MALDI-TOF main +1 ionization peak of 1:1, 1:3 and 1:5 CNDs. (B) Table for output of XPS analysis for carbon, oxygen, and nitrogen. (C) Schematic representation of radical carboxylation of CND edges.

ively. In support, the fluorescamine assay confirmed the results of FTIR by quantifying the surface -NH₂. Specifically, the number of surface groups is 0.007 mol g^{-1} , 0.010 mol g^{-1} , and 0.024 mol g^{-1} for the 1:1, 1:3, and 1:5 CND samples, respectively (Fig. 3A). Next, the zeta potential measurements revealed that the 1:1, 1:3 and 1:5 CNDs show -38.8, -23.4, and -20.4 mV, respectively (Fig. 3A). Furthermore, the formation mechanism of these CNDs should be based on two steps. The first step includes the condensation reaction between the amine groups of urea and the terminal carboxylic component of citric acid, eventually, resulting in the formation of a polyamide. These polyamide structures serve as formation seeds for the second step which involves carbonization via continuous heating. Thus, keeping the citric acid (carbon source) amount fixed should also assist in maintaining the constant formation of seeds. From this point in theory, modified CNDs

should form a similar number of seeds and then follow similar carbonization routes that finally result in a similar particle mass. MALDI-TOF main +1 ionization peaks of modified CNDs support this hypothesis by demonstrating main peaks close to 750 for all samples (Fig. 3A).

Next, XPS studies were performed to further analyze the surface functional groups of CNDs. Fig. S2† displays XPS core levels for the C 1 s, N 1 s and O 1 s orbitals of the modified CNDs. The C 1s signal shows the presence of a relatively low amount of sp² hybridized carbon (284.7 eV) for each sample that slightly increased by the increase of citric acid/urea ratio with percentages of up to 54–58% with an increment of C sp² for 1:3 and 1:5 CNDs (Fig. S2A, a, b, c†). An opposite trend was observed for carboxylic functionalities (289.7 eV C 1s, 532.7 eV O 1s) (Fig. S2A, d, e, f†). Considering the O 1s signal, a decrease in carboxylic functionality was also detectable from

Nanoscale Paper

the 1:1 to 1:3 CNDs while carbonyl residue percentages did not show any appreciable trend. The N 1s signal showed an increase of amine functions (400.1 eV) with the decrease of citric acid/urea ratio. Furthermore, an increase of pyridinic (399.4 eV) and a decrease of NQ (nitrogen species included in the graphitic plane like the heptazine structures, 401.4 eV) were observed (Fig. S2A, g, h, i†). These trends are summarized in Fig. 3B. XPS analysis of modified CNDs is crucial to understand their biological intrinsic behaviors which will be further discussed in the following sections.

The decrease of the citric acid/urea ratio led to a radical rich environment that promoted aromatic condensation as proved by the increase of sp² CNDs' carbon. The heterolytic cleavage of the C-N bond of urea did not induce the insertion of nitrogen into the aromatic plane or into the formation of biuret but as an amine group. The nitrogen rich CNDs displayed a decrease of carboxylic groups reasonably located on the edges according to the Lerf-Klinowski model.²¹ The decreased number of carboxylic groups with the decrease of citric acid/urea ratio could be explained by the radical mechanism reported in Fig. 3C. The radical rich environment could lead to an improved reactivity of exposed edges with a partial replacement of carboxylic moieties with amine through the radical formation of carbon dioxide, ammonia, and carbon monoxide. The presence of excess carbon monoxide supports the presence of a great number of carbonyl residues produced through radical insertion or the carbonyl on the edges with or without carboxylic replacement. Considering all points raised above, the increase in the amount of urea induced an increase in shell functionalities with a decrease of nitrogen doped aromatic layer. Thus, both the 1:3 and 1:5 CNDs are characterized with a more hydrophobic core and more polar external shell compared to the 1:1 CNDs.

3.2. Doxorubicin conjugation and quantification on modified CNDs

Here, we studied modified CNDs' nanocarrier properties by conjugating them with doxorubicin, an anticancer drug. It is known that doxorubicin has significant side effects towards healthy cells.²² The use of nanocarriers such as CDs should limit the side effects by achieving a targeted delivery of doxorubicin to cancer cells. We loaded doxorubicin on the surface of modified CNDs by creating carbodiimide crosslinks between the CNDs and the loading cargo. A long-established EDC/NHS bioconjugation between CNDs and doxorubicin was performed. Fig. 4A shows UV-vis absorption spectra of the purified 1:1, 1:3 and 1:5 CNDs conjugated with doxorubicin. Doxorubicin has a specific absorption at 490 nm. The same band at 490 nm appears in 1:1, 1:3, and 1:5 CNDs-Dox spectra, attesting the achievement of a successful conjugation. We quantified the loaded doxorubicin on the modified CNDs using a technique previously established in our lab.²³ This analytical tool is based on the chirality of the molecules. The working principle of circular dichroism (CDH) involves the differential absorption of left and right circularly polarized light. CNDs don't exhibit a CDH signal by themselves.

However, when a chiral molecule is conjugated on the CNDs, it can be detected with CDH. Therefore, using these features, we can create a calibration curve and calculate the amount of doxorubicin loaded on the CNDs (Fig. 4B). The drug loading amounts (Fig. 4C) were found to be 0.41, 0.51, and 0.52 µmol g^{-1} for the 1:1, 1:3, and 1:5 CNDs, respectively. This might show a rather surprising result, considering the similar amount of available -COOH sites on the surfaces of modified CNDs. However, the isoelectronic point (pI) of the molecule which donates -NH₂ groups is very important for the mechanism of EDC/NHS coupling.²⁴ Additionally, molecules with higher pI will be accepted as a base and their EDC/NHS conjugation will be decreased with highly negative structures that donate -COOH groups.²⁴ Doxorubicin's pI is 8.40.²⁵ Thus, doxorubicin is included in the category of basic structures. From this point, the 1:1 CNDs carry the highest negative surface charge compared to the 1:3 and 1:5 CNDs which may result in more repulsions of doxorubicin and lower coupling with its surface -COOH groups.

Finally, Fig. 4D presents the difference between the surface charges of modified CNDs before and after doxorubicin conjugations. As a general outcome of the occupation of surface carboxylic groups with the conjugation of doxorubicin, all modified CNDs conjugated with this drug showed a significant decrease in the negative charge of the surface. Additionally, 1:3 and 1:5 CNDs were even slightly positively charged after the doxorubicin conjugations. Last but not least, Fig. S3† shows the AFM images of modified CNDs after the conjugation with doxorubicin. In this figure, the height profile of the 1:1, 1:3 and 1:5 CND-Dox conjugates from AFM studies is in the range between 1.5 and 4.1 nm. Moreover, we have shown that 1:1, 1:3, 1:5 CNDs alone before any surface conjugations have a height profile range of 1.0-3.8 nm, 1.6-2.0 nm, and 1.3-2.1 nm, respectively. On comparing the AFM height profiles of the modified CNDs before and after doxorubicin conjugation, it can be seen that there was a slight increase in the overall size of the nanosystems upon doxorubicin conjugation.

3.3. In vitro cell viability studies

Here, we performed two separate in vitro studies with different time intervals towards a non-tumor cell line, namely MSC, and five different aggressive cancer cell lines, SJ-GBM2, KNS42, SMS-KCNR, NP53, and SF188. Nanocarriers cannot stay around the tumor site for 72 hours in a more complex environment.²⁶ Therefore, in addition to 72 hours, we included a shorter treatment period of 3 hours to mimic a more realistic scenario. Moreover, as discussed previously, original 1:1 CNDs have shown a selective cancer cell uptake towards a glioblastoma cell line, named SJ-GBM2.10 To further study this selective cancer cellular uptake towards SJ-GBM2, we applied more studies and collected data for our modified CNDs with this cell line. Additionally, we wanted to expand our studies to include additional pediatric high-grade glioma (KNS42, NP53, and SF188) and neuroblastoma (SMS-KCNR) cell lines to examine the cancer selective uptake of modified CNDs. Since myc oncoproteins are known to drive glutamine uptake and

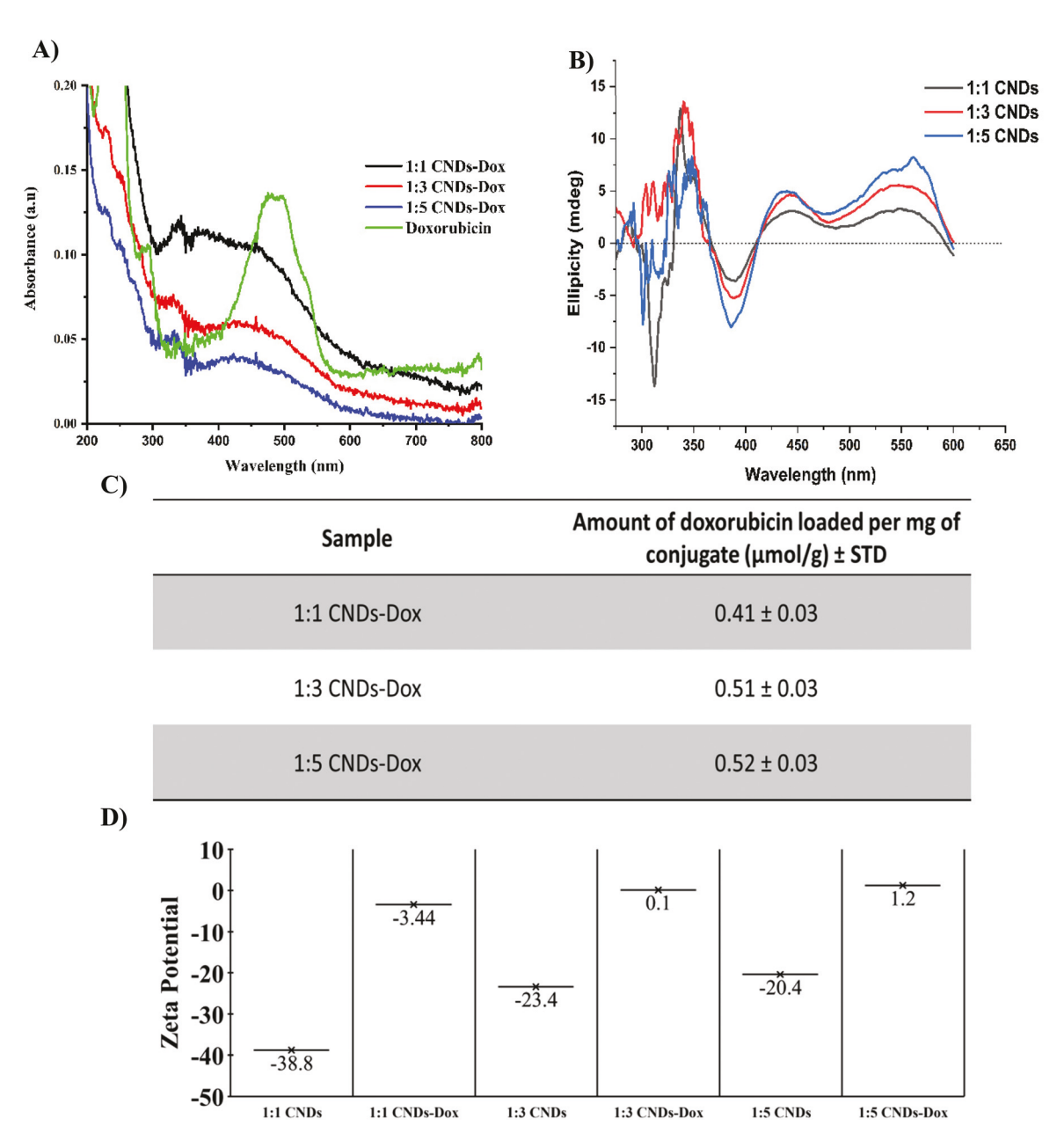


Fig. 4 (A) UV-vis absorption spectra of Dox, 1:1 CND-Dox, 1:3 CND-Dox and 1:5 CND-Dox conjugates. (B) Circular dichroism (CD) spectra of 1:1 CND-Dox, 1:3 CND-Dox and 1:5 CND-Dox conjugates. (C) Table for the amount of doxorubicin loaded per mg of each conjugate. (D) Table for comparing the differences between zeta potential (surface charge) measurements of surface modified CNDs before and after doxorubicin conjugation.

metabolism in cancer cells, we specifically included c-myc amplified SF188 and n-myc amplified KNS42 and SMS-KCNR cell lines. ^{27–30} Both the 1:3 and 1:5 CNDs–DOX conjugates do not have significant change in the 3 hour cell viabilities towards non-tumor MSC cells when compared to the 1:1 CNDs (Fig. 5A). Moreover, the 1:3 and 1:5 CNDs–DOX conjugates showed notable anticancer efficacy towards four glioblastoma cell lines: SF188, NP53, KNS42, and SJ-GBM2, and one neuroblastoma, SMS-K-CNR (Fig. 5A). 1:3 CNDs, conversely, achieved the best anticancer efficacy among the three modified CNDs–Dox conjugates. The IC₅₀ values of 1:3 CNDs were as

low as 105.6 nM (Fig. 5B). For most cases, 1:3 CNDs-Dox anticancer efficacies were better than the toxicity of doxorubicin alone (Fig. 5B and C). We observed that all cell lines exhibited traditional dose dependent inhibition log curves (Fig. S4A†). Subsequently, the same cytotoxicity experiments were performed for 72 hours (Fig. 6A). Due to the initiation of passive diffusion after a significant period of time, CNDs start to get in with passive cellular uptake pathways such as endocytosis. Therefore, we have observed higher toxicity for all modified CNDs-Dox conjugates and doxorubicin for the 72 hour treatment. Additionally, when we compare the viability results of

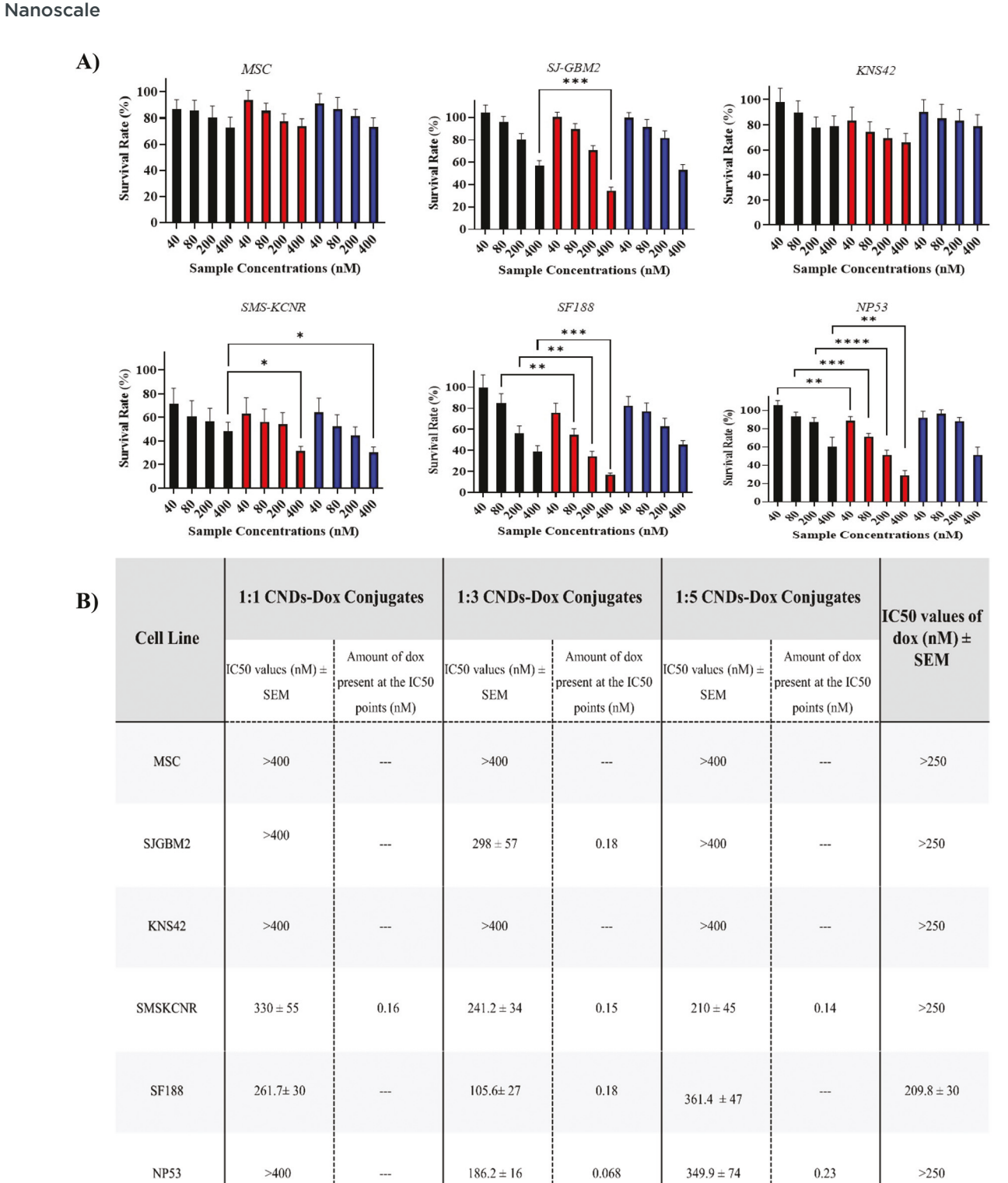


Fig. 5 (A) Results of 3 hour exposure cell viability assay of 1:1 CND-Dox (black), 1:3 CND-Dox (red) and 1:5 CND-Dox (blue) conjugates (B) table for IC₅₀ values and amount of dox present at the IC₅₀ points of CND-Dox conjugates, and IC₅₀ values of doxorubicin alone. Results are expressed as % of the survival rate. Values are means (nM) \pm SEM (n = 12). P was accepted as 0.05.

the 1:1 CNDs with the 1:3 and 1:5 CNDs, we did not observe a significant change in biocompability. From the same perspective, it was not surprising to see much higher anticancer efficacy of the modified CNDs-Dox conjugates towards the cancer cell lines (Fig. 6A). Regarding the IC_{50} values of the 72 hour treatments, 1:3 CNDs-Dox conjugates generated results as low as 32.8 nM (Fig. 6B). Similarly, all cell lines demonstrated traditional dose dependent inhibition log curves

Paper Nanoscale

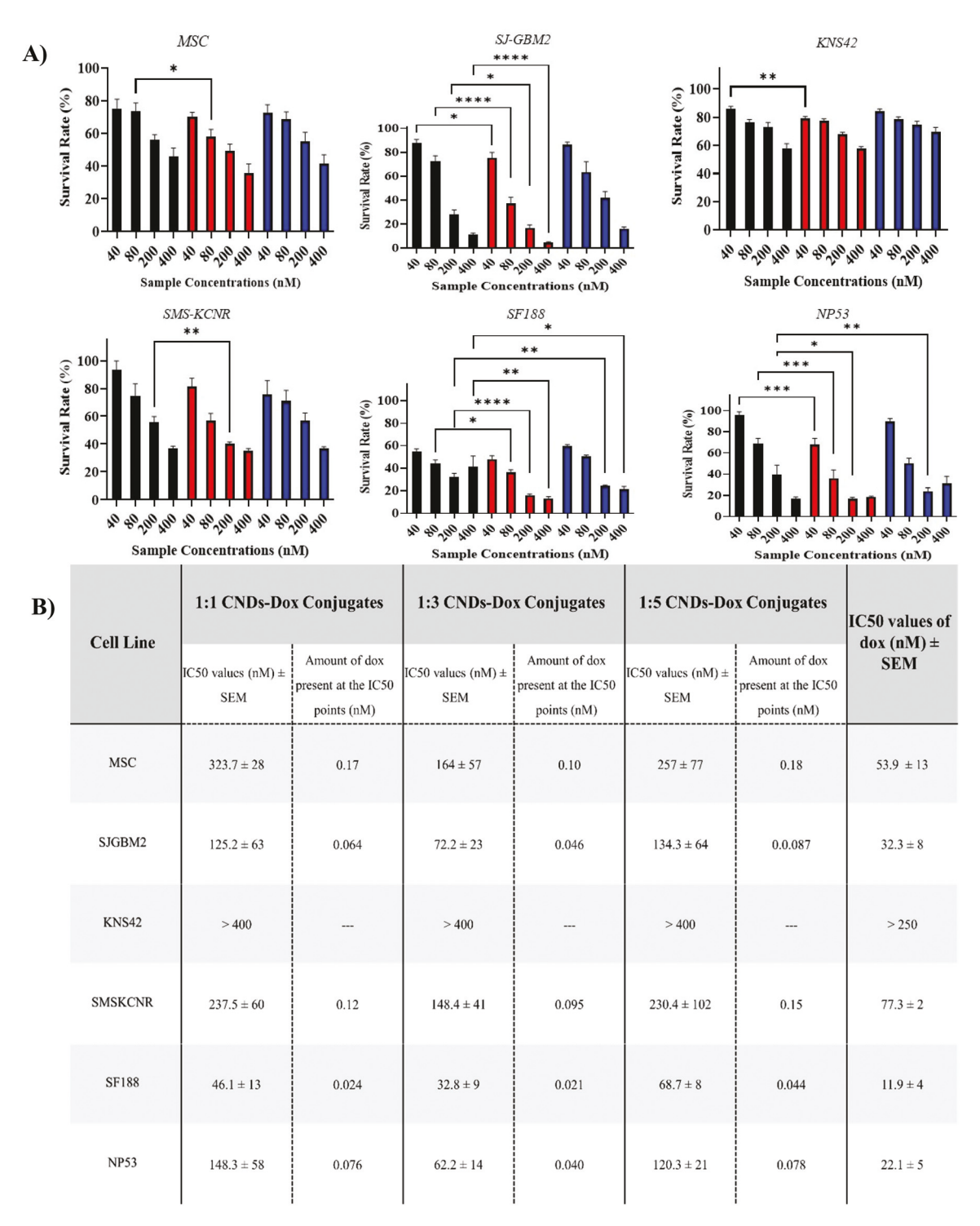


Fig. 6 (A) 72 hours exposure cell viability results of 1:1 CNDs–Dox (black), 1:3 CNDs–Dox (red) and 1:5 CNDs–Dox (blue) conjugates (B) table for IC_{50} values and amount of dox present at the IC_{50} points of CNDs–Dox conjugates, and IC_{50} values of doxorubicin alone. Results are expressed as % of survival rate. Values are means (nM) \pm SEM (n = 12). P was accepted as 0.05.

(Fig. S4B†). Finally, we calculated the amount of doxorubicin present on the IC_{50} concentrations of CNDs-Dox conjugates (Fig. 6C). With more precise cancer cell delivery of much lower concentrations of doxorubicin, we succeed to obtain not only improved anti-cancer efficacy but also reduced side effects to

non-tumor cells. To sum up, the 1:3-CNDs-Dox conjugates showed the highest anticancer efficacies for most cases at the concentrations tested. 1:5 CNDs-Dox conjugates carry higher numbers of doxorubicin on their surface, but the 1:3-CND-Dox conjugates showed better anti-cancer efficacy. Therefore, we

Nanoscale

hypothesize that because there is a difference in their cellular uptake mechanisms, the modified CNDs-Dox conjugates produced different anticancer efficacies. To support our hypothesis, we performed both western blotting and bioimaging studies.

3.4. Western blot analysis

We tested the transporter expression levels on the 6 cell lines for ASCT2 and LAT1 transporters. We chose ASCT2 and LAT1 transporters for western blotting since the ASCT2 and the LAT1 transporters are the most common highly expressed transporters on large populations of cancer cells and CND surface functional groups resemble ASCT2 and LAT1 amino acids.31 Briefly, the amino acid recognition mechanism of ASCT2 is based on the exchange of small amino acids via the variation in the concentration of the Na⁺ ion in the outer cellular microenvironment.32 On the other hand, LAT1 transporter's amino acid recognition is independent of both the Na⁺ ion concentration and the pH of the outer cell microenvironment. LAT1 transporters form a heterodimeric complex with the glycoprotein 4F2hc to import amino acids. 33 Fig. S5A† presents our western blot analysis for these two transporters on the cell lines that have been employed for cytotoxicity.

Firstly, all modified CNDs-Dox conjugates had poor anticancer effects for the KNS42 cell line (Fig. 5B and 6B). If we correlate these data with our western blot analysis, we can see that the KNS42 cell line does not express high levels of the ASCT2 and LAT1 transporters which may result in low cellular uptake for our CND-Dox conjugates (Fig. S5A†). The SI-GBM2, SF188 and SMS-KCNR cell lines on the other hand express high levels of ASCT2 transporters which can lead to higher cellular uptake and anticancer efficacy for the 1:3 CND-Dox conjugates. Moreover, if we look at the cases where LAT1 expression level is appreciable such as for the SMS-KCNR cell line, we observed that the anticancer efficacy of the 1:5-CND-Dox conjugates improves. Considering both the western blot studies and cytotoxicity results, we hypothesized that the 1:1 and 1:3-CNDs are more prone to be transported by both the ASCT2 and the LAT1 transporters while the 1:5 CNDs tend to enter cells through LAT1 transporters (Fig. S5B†). The amino acid recognition mechanisms of these two transporters also support our hypothesis. For instance, the ASCT2 transporter recognizes amino acids that resemble glutamine, alanine, and threonine which possess functional groups including -COOH, -NH2, and -OH on their structure. 1:1 and 1:3 CNDs have these func-

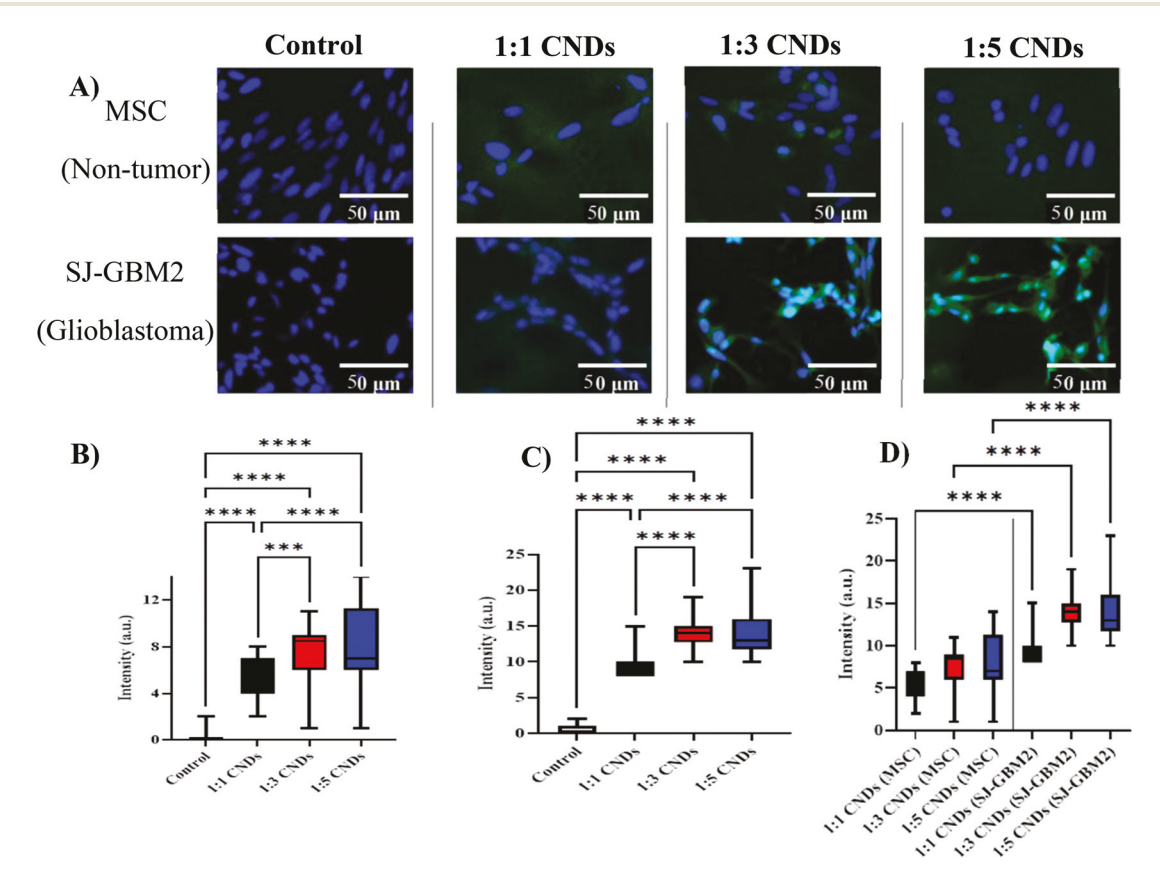


Fig. 7 (A) Fluorescence microscopy images of MSC (non-tumor) and SJ-GBM2 (glioblastoma) cells treated with 1:1, 1:3, and 1:5 CNDs. Both cell lines were treated with 1 mM concentration of modified CNDs for 1 h. Scale bars are 50 µm. Excitation wavelength: blue, 358 nm, green, 488 nm. (B) Green PL intensity quantification for MSC (non-tumor) images of modified CNDs. Values are means ± range (n = 30). (C) Green PL intensity quantification for SJ-GBM2 (glioblastoma) images of modified CNDs. Values are means + range (n = 30). (D) One-way (ANOVA) statistical comparison for MSC (non-tumor) and SJ-GBM2 (glioblastoma) green PL intensity of modified CNDs. Values are means + range (n = 30). *P < 0.05, **P < 0.01, ****P < 0.0001. In boxplots, center bars represent medians and expand to the first and third quartiles; whiskers extend to min/max data points.

Paper Nanoscale

tional groups, especially -OH, on their surface. On the other hand, the LAT1 transporter recognizes amino acids by forming dimeric complex structures with membrane glycoproteins. All modified CNDs carry significant amounts of -COOH and -NH2 groups to be recognized as one of the LAT1 transporter amino acids such as phenylalanine, tryptophan, and tyrosine. We further tested our claim about the cellular uptake mechanisms for 1:1, 1:3 and 1:5 CNDs with in vitro bioimaging studies.

3.5. *In vitro* bioimaging

In this paper, in addition to performing imaging studies with modified CNDs, we have designed bioimaging studies to assess the uptake mechanisms of these CNDs. We first demonstrated bioimaging studies of the modified CNDs using a nontumor cell line, MSC, and a glioblastoma cancer cell line, SJ-GBM2. Control groups have shown that there was no PL leakage from blue to green channels or vice versa. Here, the green channel was attributed for observation of modified CNDs, and the blue channel was assigned for inspection of Hoechst nucleus staining dye. The modified CND treatment did not affect the cell morphology and viability. As can be seen from Fig. 7A, 1:3 and 1:5 CNDs were able to keep the same trait as 1:1 CNDs by selectively entering cancer cells at higher rates. 1:3 CNDs illustrated the significant increase in the green PL intensity for both the MSC and SJ-BM2 cell lines compared to 1:1 CNDs (Fig. 7B-D). Meanwhile, the 1:5 CNDs also

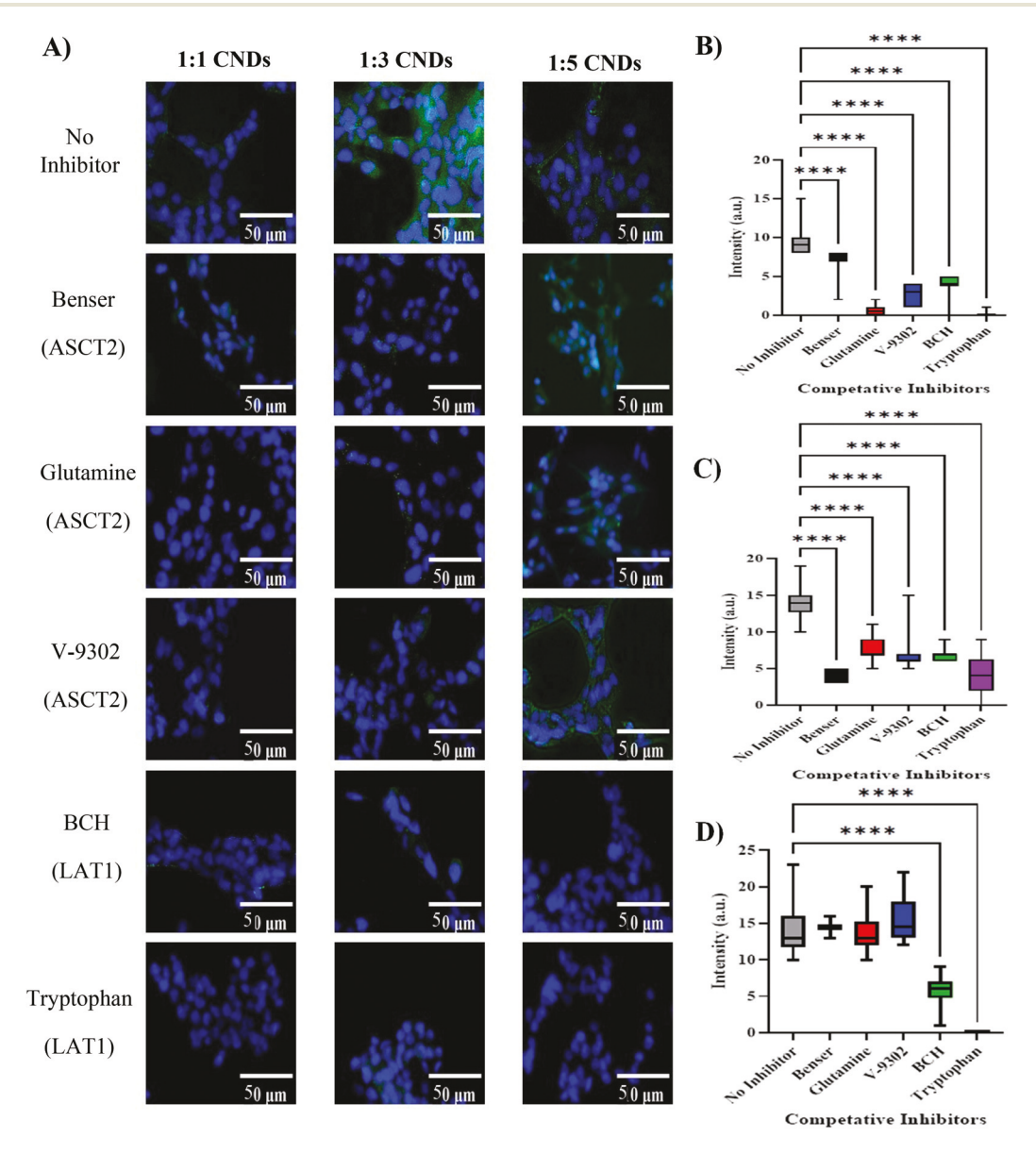


Fig. 8 (A) Fluorescence microscopy images of SJ-GBM2 (glioblastoma) cells treated for an hour with 1 mM 1:1, 1:3 and 1:5 CNDs, 60 mM Benser, 60 mM glutamine, 15 μM V-9302, 15 mM BCH, and 60 mM tryptophan. Scale bars are 50 μm. Excitation wavelength: blue, 358 nm, green, 488 nm. (B, C, D) Green PL intensity one-way (ANOVA) quantification of 1:1, 1:3 and 1:5 CNDs, respectively. Values are means \pm range (n=30). P was accepted as 0.001. *P < 0.05, **P < 0.01, ****P < 0.0001. In boxplots, center bars represent medians and expand to the first and third quartiles; whiskers extend to min/max data points.

Nanoscale Paper

displayed significant PL brightness compared to the 1:1 CNDs for both the non-tumor and cancer cell bioimaging (Fig. 7B-D). To further investigate cellular uptake properties of the modified CNDs, we implemented bioimaging studies with the presence of the ASCT2 and the LAT1 transporters' competitive ligands (Fig. 8A). We selected five competitive inhibitor ligands to work: Benser, glutamine, V-9302, BCH, and tryptophan. It has been assessed in previous studies that cellular uptake mechanisms of competitive inhibitors of Benser, glutamine, and V-9302 are directly related to the ASCT2 transporter levels.34-36 Further studies have shown that BCH and tryptophan are taken up by the LAT1 transporter on the cells. 37,38 We hypothesized that if the possible cell uptake mechanism of 1:1, 1:3 and 1:5 CNDs is connected with the ASCT2 and the LAT1 transporters, then their PL intensity for bioimaging should be affected in the presence of the competitive molecules that occupy the same transporters for cellular uptake. Therefore, we quantified the PL intensity of the modified CNDs that are treated with glioblastoma (SJ-GBM2) cells with and without the presence of inhibitors. The PL intensities of images were calculated using ImageJ software, and the results were analyzed by the one-way ANOVA statistical technique. The SJ-GBM2 cells were treated in the same manner as the previous imaging study except for the addition of competitive inhibitors to the same cell media. The treatment of modified CNDs and inhibitor solutions did not change the morphology and viability of the cells (Fig. S5†). Firstly, the original 1:1 CNDs' PL intensity was affected in the presence of both ASCT2 and LAT1 transporters' competitive molecules (Fig. 8B). Therefore, there is a possibility that the 1:1 CNDs are also prone to be taken up by both the ASCT2 and LAT1 transporters. Furthermore, with the presence of the ASCT2 and the LAT1 transporter inhibitors, the PL intensity of the 1:3 CNDs also decreased (Fig. 8C). In other words, the 1:3 CNDs are prone to using both the ASCT2 and the LAT1 transporters to enter the cancer cells, so the presence of one of the competitive inhibitors reduced their uptake. For the case of the 1:5 CNDs, we observed complete inhibition of the PL intensity with the presence of the LAT1 transporter inhibitors (Fig. 8D). Meanwhile, the presence of ASCT2 transporter inhibitors did not affect PL intensity of the 1:5 CNDs (Fig. 8D).

In addition, it is well known that for passive endocytic cell uptake nanoparticles with positive charge are more preferred compared to negatively charged particles. Meanwhile, in active cell uptake routes the interactions of transporters' ligand binding site with particles determine the cellular uptake rates.³⁹ It has been shown that after the doxorubicin conjugation all of the modified CNDs exhibited a significant increase in the surface charge. From the previous statement, we can interpret that their cellular uptake rates via passive routes may be enhanced. On the other hand, our in vitro bioimaging studies suggest that superior cancer selective uptake and directly better anti-cancer efficacies of 1:3 CNDs and 1:3 CNDs-Dox nano systems are also highly linked with the interaction between the transporters' ligand binding site and the modified CNDs through active cellular uptake routes.

The majority of existing CDs in the literature lack studies about their cellular uptake mechanism. 40 Additionally, papers which discuss the cellular uptake of current CDs emphasize highly on the passive routes instead of active routes. 41,42 Therefore, this study provides elaborate information about not only the passive routes, but also the active pathways.

To summarize, we hypothesized that the possible cellular uptake mechanism of the 1:1, 1:3 and 1:5 CNDs changed with the modifications of their surface structural groups. In particular, the 1:1 and 1:3 CNDs tend to penetrate the cells through both ASCT2 and LAT1 transporters due to having surface functional groups such as primary amines, carboxylic groups, and alcohol groups that resemble small amino acids. On the other hand, the 1:5 CNDs carry more N pyridinic groups (and lack -OH groups) on their surface which resemble large amino acids and prefer the LAT1 pathway.

Conclusions

Here, we have successfully synthesized surface modified CNDs by changing the precursor ratios. Our characterization results have shown that an increase in the amount of urea as a precursor also increases the amount of surface -NH2 groups in addition to a decrease of -COOH groups. Modified CNDs were meticulously characterized to assess their optical, size and morphology, surface functional groups and surface charge properties. We performed a carbodiimide coupling with doxorubicin to use these modified CNDs as nanocarriers. Due to the favorable surface charges, we were able to load more doxorubicin on 1:3 and 1:5 CNDs. Next, the CND-Dox conjugates were applied on 6 distinct cell lines for in vitro viability studies. Both 3 and 72 hours of treatments have shown that the biocompatibility of the 1:3 and 1:5 CND-Dox did not change compared to 1:1 CND-Dox towards the non-tumor cell line. On the other hand, the 1:3 and 1:5 CND-Dox conjugates showed significantly better anticancer efficacy against most of the cancer cells. In particular, the 1:3 CND-Dox conjugates showed improved anticancer efficacy for some cases compared to doxorubicin alone. We were able to introduce less doxorubicin but still acquire better anticancer efficacy with the CND-Dox conjugates. We hypothesized that having significant anticancer effects on some cancer cell lines but not all of them could be related to the possible cellular uptake mechanism of the modified CNDs. Hence, we performed western blotting studies on the cell lines that have been employed to measure the expression levels of two common cancer cell transporters: ASCT2 and LAT1. According to western blotting, there is an alignment between the anti-cancer efficacy of CND-Dox conjugates and expression levels of ASCT2 and LAT1 transporters on the cell lines tested. Next, in vitro bioimaging studies were applied to further investigate the effects of surface functional groups on the cellular uptake of CNDs. Both the 1:3 and the 1:5 CNDs were able to maintain selective cancer cellular uptake. In addition, they exhibit significantly higher PL intensities compared to the original 1:1 CNDs. Finally, we introduced five competitive ligands of ASCT2 and LAT1 into the CND bioimaging environment to assess changes in the PL intensity of the CNDs. PL intensities of both 1:1 and 1:3 CNDs were decreased in the presence of both ASCT2 and LAT1 transporter inhibitors. However, only LAT1 transporter inhibitors were able to significantly weaken the PL intensity of the 1:5 CNDs. Our studies suggest that the possible cellular uptake mechanism of 1:1 and 1:3 CNDs is linked to ASCT2 and LAT1 transporters. Consequently, 1:5 CNDs are prone to be taken up by LAT1 transporters of the cells. This study provides a chemical and biological foundation for understanding the effects of surface functional groups of nanocarriers on their cellular uptake mechanism. For future applications, this study opens a novel door for building personalized nanomedicine for specific cancer types by the effects of the surface functional groups.

Author contributions

E. K. C. designed and performed experiments, analyzed data, and wrote the paper; M. S. and F. A. V. helped with the in vitro studies. J. M. G. assisted in the synthesis of CNDs; M. B. and A. T. performed XPS studies and build the reaction scheme for the structure of CNDs; S. V. contributed to the revision of the manuscript; R. M. G. and R. M. L. supervised the experiments and edited the manuscript; all authors discussed the results and implications and commented on the manuscript at all stages.

Conflicts of interest

There are no conflicts to declare.

Acknowledgements

R. M. L. thanks the support from National Science Foundation under the grant 1809060 and 2041413. R. M. G. gratefully acknowledges the support of the BCURED Foundation, the Florida Department of Health Live Like Bella research grant 21L08 and the Mystic Force Foundation. Also, authors gratefully acknowledge the great support from University of Miami, USA.

References

- 1 Y. Wang, Y. Zhu, S. Yu and C. Jiang, Fluorescent carbon dots: rational synthesis, tunable optical properties and analytical applications, RSC Adv., 2017, 7, 4973–4989.
- 2 M. A. Issa, et al., Fluorescent recognition of Fe3+ in acidic environment by enhanced-quantum yield N-doped carbon dots: optimization of variables using central composite design, Sci. Rep., 2020, 10, 11710-11710.

- 3 L. Li and T. Dong, Correction: Photoluminescence tuning in carbon dots: surface passivation or/and functionalization, heteroatom doping, J. Mater. Chem. C, 2019, 7, 315-315.
- 4 N. Esfandiari, et al., Effect of carbonization degree of carbon dots on cytotoxicity and photo-induced toxicity to cells, Heliyon, 2019, 5, e02940-e02940.
- 5 S. Hassan, et al., Evolution and clinical translation of drug delivery nanomaterials, Nano Today, 2017, 15, 91-106.
- 6 D. A. Fenstermacher, R. M. Wenham, D. E. Rollison and W. S. Dalton, Implementing personalized medicine in a cancer center, Cancer J., 2011, 17, 528-536.
- 7 Confirmation hearings on the nominations of Thomas Perrelli, nominee to be Associate Attorney General of the United States and Elena Kagan, nominee to be Solicitor General of the United States: hearing before the Committee on the Judiciary, United States Senate, One Hundred Eleventh Congress, first session, February 10, 2009. (U.S. G.P.O., 2009).
- 8 J. W. Neal, et al., Erlotinib, cabozantinib, or erlotinib plus cabozantinib as second-line or third-line treatment of patients with EGFR wild-type advanced non-small-cell lung cancer (ECOG-ACRIN 1512): a randomised, controlled, open-label, multicentre, phase 2 trial, Lancet Oncol., 2016, 17, 1661-1671.
- 9 B. J. Druker, et al., Five-Year Follow-up of Patients Receiving Imatinib for Chronic Myeloid Leukemia, N. Engl. J. Med., 2006, 355, 2408-2417.
- 10 P. Y. Liyanage, et al., Carbon Nitride Dots: A Selective Bioimaging Nanomaterial, Bioconjugate Chem., 2019, 30, 111-123.
- 11 E. R. Still and M. O. Yuneva, Hopefully devoted to Q: targeting glutamine addiction in cancer, Br. J. Cancer, 2017, 116, 1375-1381.
- 12 C. Lopes, C. Pereira and R. Medeiros, ASCT2 and LAT1 Contribution to the Hallmarks of Cancer: From a Molecular Perspective to Clinical Translation, Cancer, 2021, 13, 203.
- 13 K. G. Halvorson, et al., A high-throughput in vitro drug screen in a genetically engineered mouse model of diffuse intrinsic pontine glioma identifies BMS-754807 as a promising therapeutic agent, PLoS One, 2015, 10, e0118926e0118926.
- 14 Y. Zhou, et al., Photoluminescent Carbon Dots: A Mixture of Heterogeneous Fractions, ChemPhysChem, 2018, 19, 2589-2597.
- 15 E. Kirbas Cilingir, et al., Metformin derived carbon dots: Highly biocompatible fluorescent nanomaterials as mitochondrial targeting and blood-brain barrier penetrating biomarkers, J. Colloid Interface Sci., 2021, 592, 485–497.
- 16 R. M. Graham, et al., Resveratrol augments ER stress and the cytotoxic effects of glycolytic inhibition in neuroblastoma by downregulating Akt in a mechanism independent of SIRT1, Exp. Mol. Med., 2016, 48, e210-e210.
- 17 B. van Dam. al., **Excitation-Dependent** Photoluminescence from Single-Carbon Dots, Small, 2017, 13, 1702098.

Nanoscale Paper

- 18 K. J. Mintz, Y. Zhou and R. M. Leblanc, Recent development of carbon quantum dots regarding their optical properties, photoluminescence mechanism, and core structure, Nanoscale, 2019, 11, 4634-4652.
- 19 V. Țucureanu, A. Matei and A. M. Avram, FTIR Spectroscopy for Carbon Family Study, Crit. Rev. Anal. Chem., 2016, 46, 502-520.
- 20 X. Cao, et al., A facile microwave-assisted fabrication of fluorescent carbon nitride quantum dots and their application in the detection of mercury ions, Spectrochim. Acta, Part A, 2015, 151, 875-880.
- 21 A. Lerf, H. He, T. Riedl, M. Forster and J. Klinowski, 13C and 1H MAS NMR studies of graphite oxide and its chemically modified derivatives, Solid State Ionics, 1997, 101, 857-862.
- 22 U. Kanwal, et al., Advances in nano-delivery systems for doxorubicin: an updated insight, J. Drug Targeting, 2018, 26, 296-310.
- 23 B. C. L. B. Ferreira, P. Y. Livanage and R. M. Leblanc, Drug Loading of Anthracycline Antibiotics on Carbon Dots Using Circular Dichroism Spectrometry, Anal. Chem., 2021, 93, 14773-14777.
- 24 X. Yang, et al., Hyaluronic acid/EDC/NHS-crosslinked green electrospun silk fibroin nanofibrous scaffolds for tissue engineering, RSC Adv., 2016, 6, 9972-99728.
- 25 G. García Rubia, et al., pH-Dependent Adsorption Release Doxorubicin on MamC-Biomimetic Nanoparticles, Langmuir, 2018, 34, 13713-13724.
- 26 Y. H. Bae and K. Park, Targeted drug delivery to tumors: Myths, reality and possibility, J. Controlled Release, 2011, **153**, 198–205.
- 27 R. M. Graham, et al., Resveratrol augments ER stress and the cytotoxic effects of glycolytic inhibition in neuroblastoma by downregulating Akt in a mechanism independent of SIRT1, Exp. Mol. Med., 2016, 48, e210e210.
- 28 L. Bjerke, et al., Histone H3.3. mutations drive pediatric glioblastoma through upregulation of MYCN, Cancer Discovery, 2013, 3, 512-519.
- 29 J. Trent, et al., Evidence for Rearrangement, Amplification, and Expression of c-myc in a Human Glioblastoma, Proc. Natl. Acad. Sci. U. S. A., 1986, 83, 470-473.

- 30 V. Tambay, V.-A. Raymond and M. Bilodeau, MYC Rules: Leading Glutamine Metabolism toward a Distinct Cancer Cell Phenotype, Cancer, 2021, 13, 4484.
- 31 B. C. Fuchs and B. P. Bode, Amino acid transporters ASCT2 and LAT1 in cancer: Partners in crime?, Semin. Cancer Biol., 2005, 15, 254-266.
- 32 L. Pochini, M. Scalise, M. Galluccio and C. Indiveri, Membrane transporters for the special amino acid glutamine: structure/function relationships and relevance to human health, Front. Chem., 2014, 2, 61-61.
- 33 J. Zhang, et al., Review of the Correlation of LAT1 With Diseases: Mechanism and Treatment, Front. Chem., 2020, 8, 564809-564809.
- 34 M. van Geldermalsen, et al., Benzylserine inhibits breast cancer cell growth by disrupting intracellular amino acid homeostasis and triggering amino acid response pathways, BMC Cancer, 2018, 18, 689-689.
- 35 M. van Geldermalsen, et al., ASCT2/SLC1A5 controls glutamine uptake and tumour growth in triple-negative basallike breast cancer, Oncogene, 2016, 35, 3201-3208.
- 36 M. L. Schulte, et al., Pharmacological blockade of ASCT2dependent glutamine transport leads to antitumor efficacy in preclinical models, Nat. Med., 2018, 24, 194-202.
- 37 D. Cibrian, et al., Erratum: CD69 controls the uptake of L-tryptophan through LAT1-CD98 and AhR-dependent secretion of IL-22 in psoriasis, Nat. Immunol., 2016, 17,
- 38 R. Yan, et al., Mechanism of substrate transport and inhibition of the human LAT1-4F2hc amino acid transporter, Cell Discovery, 2021, 7, 16-16.
- 39 M. Saadat, et al., Drug Targeting Strategies Based on Charge Dependent Uptake of Nanoparticles into Cancer Cells, J. Pharm. Pharm. Sci., 2019, 22, 191-220.
- 40 C. Fu, K. Qian and A. Fu, Arginine-modified carbon dots probe for live cell imaging and sensing by increasing cellular uptake efficiency, Mater. Sci. Eng., C, 2017, 76, 350-355.
- 41 Y. Wei, X. Jin, T. Kong, W. Zhang and B. Zhu, The endocytic pathways of carbon dots in human adenoid cystic carcinoma cells, Cell Proliferation, 2019, 52, e12586.
- 42 A. Halder, et al., One-Pot Green Synthesis of Biocompatible Graphene Quantum Dots and Their Cell Uptake Studies, ACS Appl. Bio Mater., 2018, 1, 452-461.